Journal of Computational Applied Mechanics 2025, 56(1): 170-195
DOI: 10.22059/jcamech.2024.387768.1324

RESEARCH PAPER

Heat Transfer Characteristics of Hybrid Nanoparticles in Newtonian Fluid inside a Channel with Air foil-shaped: A CFD Simulation using COMSOL Multiphysics

A. Zeeshan [a, b], R. Ellahi [a, c, *], Sadiq M. Sait [d, e], Shah Nawaz Sharif [a]

[a] *Department of Mathematics & Statistics, International Islamic University Islamabad Pakistan*
[b] *Department of Mathematics, College of Science, Korea University, 145 Anam-ro, Seongbuk-gu, Seoul 02841, Republic of Korea*
[c] *Center for Modeling & Computer Simulation, Research Institute, King Fahd University of Petroleum & Minerals, Dhahran, Saudi Arabia*
[d] *Department of Computer Engineering, King Fahd University of Petroleum & Minerals, Dhahran, Saudi Arabia*
[e] *Interdisciplinary Research Center for Smart Mobility and Logistics, King Fahd University of Petroleum & Minerals, Dhahran, Saudi Arabia*

Abstract

Current study aims to investigate flow and heat transfer in a converging diverging Channel for compressible Nanofluid. An airfoil-shaped steel fragment is used as an internal obstetrical before flow enters to assess its impact on flow behavior and heat transfer. For Nanofluids in-compressible Newtonian fluid is assumed as a base fluid. Hybrid Nanofluid model is applied to develop the governing flow equation. The computational fluid dynamics tool i.e. COMSOL Multiphysics is applied to simulate a variety of boundaries including inlet and outlet conditions, no-slip and slip conditions etc. A triangular mesh is created using COMSOL Multiphysics. The contour plot of momentum and thermal boundary layer are examined. The effects of the contraction and the steel fragment on the fluid's velocity, pressure, temperature and convection of heat are also addressed.

Keywords: Heat transfer, nanoparticles, Newtonian fluid, viscous dissipation, Airfoil-shaped, COMSOL Multiphysics

1. Introduction

Nanofluids are made up of homogeneously distributed specially generated Nano-sized particles having size ranging from 1 to 100nm. Common base fluids include water, motor oil, biofluids, and organic fluids. Various forms of carbon, metals, and their oxide are frequently used as the nano-particles. The applications of nanofluid have disclosed hug potential of nanofluid with engineering applications. The pioneering research into the thermal performance enhancements of nanofluids was conducted by Choi and Eastman [1]. The significance of nanofluid can be seen in [2-14]. Numerous scholars examined the effects of fluid structure, concentration, size, and other factors on thermal efficiency. It is well documented that the addition of solid nanosized particles to base fluids enhances the fluid's thermal conductivity and heat transfer rates when compared to ordinary fluids, therefore, a surge of interest arises in nanofluids from the scientists cross the

*Corresponding author (R. Ellahi): E-mail: rahmatellahi@yahoo.com

globe. Yan et al. [15] investigated the rheological behavior of nanoparticles by an experimental study. Mahabaleshwar et al. [16] examined boundary layer flow of non-Newtonian fluid with carbon nano-tubes and heat transport phenomena over a sheet.

Blood vessels are an essential part of circulatory system. The circulatory system's main purpose is to provide active tissues with oxygen and other nutrients while also getting rid of waste materials. Arterial stenoses are narrowing arteries that may get worse over time and restrict the flow of blood to the organ systems and may leads to death. Substantial theoretical work has been done to understand how substrate concentration affects blood flow through a stenosed artery. Aneurysms and stenosis are examples of arterial diseases that can significantly modify the attribute of blood flowing through the arteries. Lipid accumulation within the vascular system may lead to the highly common development of stenosis in blood vessels. An artery develops stenosis due to development of lesion that extend into the lumen. One of the worst effects of this restriction when an artery of that type develops stenosis is an increase in resistance and, consequently, a decrease in blood flow through the artery. Hence, the development of stenosis may lead to severe arterial and cardiovascular issues. Shojaie Chahregh and Dinarvand [17] studied the flow of blood-based nanofluids through an artery with Ti2O-Ag nanoparticle, focusing on applications in the cardiovascular system and acute respiratory conditions. Shahzadi and Bilal [18] explored the impact of penetration on blood flow for nanofluids in bifurcated stenosed arteries. Basha et al. [19] investigated bio-nanofluid flow in an artery using finite difference computation. The similar study addressed to fascinate the phenomena of blood flow effects [20, 21].

Due to their photo-optical properties, gold nanoparticles have shown to be effective tools in a range of uses for nanomedical application. Research on and application of gold nanoparticles in bioengineering and biomedicine are currently very common. The use of gold nanoparticles is expanding in the fields of biology, delivery of medicines, cancer treatment, immunological modulation, implants, and prosthetics of lab on chip studies. In general, biological systems are inert and stable. Moreover, small concentrations of gold nanoparticles don't seem to be harmful. Gold nanoparticles may be applied to physiological therapy, health, and diagnostics. Research is still ongoing on the application of gold nanoparticles in treatment of vascular diseases. Plasmatic UV thermal treatment and the infusion of gold via an on-artery patch were found to reduce the amount of plaque in a 180-person clinical study. The blood flow of metallic nanoparticles via stenosed artery have not yet been investigated through mathematical equations. Azmi et al. [22] investigated unsteady boundary layer flow of natural convection of non-Newtonian fluid in a cylinder. Waqas et al. [23] demonstrated how the form factor affected the hybrid nanofluid containing nanoparticles. Elnaqeeb et al. [24] investigated the blood flow in a narrowed stenosed tube with varying nanofluid viscosity, focusing on the hemodynamic properties of gold nanoparticles. Khan et al. [25] examined the impact of a magnetic field on Sisko fluid flow containing metallic nanoparticles over a porous curved surface, considering the effects of radioactivity and partial slip.

An effective simulation program utilized in many branches of research, engineering, and physics is called COMSOL Multiphysics. Its main job is to solve coupled systems of PDEs in complex Multiphysics issues. Mimics how electrical systems might behave in both static and dynamic scenarios examine the relationship between a material's mechanical, thermal, and electromagnetic properties utilized in educational settings to instruct students in difficult physics, engineering, and arithmetic concepts. By integrating these several applications into a single platform, COMSOL Multiphysics enables users to create models that incorporate a variety of physical phenomena and their interactions. Because of its adaptability, it is a priceless instrument for carrying out cutting-edge scientific research and resolving real-world engineering issues. Salvi et al. [26] examined that despite using a coarser mesh size due to storage constraints, the thermodynamic values predicted for the CMC outcome ($R2 = 0.9$) and tap water ($R2 = 0.85$) were quite accurate. Sezgin et al. [27] investigated COMSOL Multiphysics simulation of an extreme temperature PEM fuel cell. It is believed that the model has a single flow channel. The Fuel Cells & Batteries Modules of licensed COMSOL Multiphysics 5.0 is used to run the experiment. The purpose of this review is to provide an overview of the most recent developments in major categories of microfluidic computations and use of several COMSOL simulations, particularly in the field of biomedical engineering. Adam and Hashim [28] studied the overview of the most recent advancements in the use of multiple COMSOL simulations and important categories of microfluidic computations, especially in the field of biomedical engineering. Maliki et al. [29] investigated two-dimensional unsteady boundary layer flow of heat and mass transport phenomena in a porous media. They used COMSOL Multiphysics 5.4 to simulate a computational approach using the least squares method for finite elements

analysis. It was discovered that, for Re = 700, the percentage fluctuation of pressure and velocity before and after the cylinder alters their behavior. Salem and Tuchin [30] investigated the patterns of blood flow are crucial to a diagnosis and management of cardiovascular disorders. Blood flow modeling has been used extensively in the past few years to gain a better understanding of the range of symptoms associated with various disorders. Wijayanti et al. [31] explored the physical characteristics of wood parts were significantly influenced by their chemical makeup. Because of its characteristics, bamboo had the greatest temperature distribution among the biomass feedstocks in the experiment. Hussain et al. [32] examined the temperature peaks at the edges, but as one moves across the top to the bottom border, it steadily rises. Maximum isothermal contour shapes are seen close to the walls, and a progressive decline in the drag coefficient is noted. Ganie et al. [33] examined five horizontal lines have been used to evaluate various fluidic and thermal properties. They discovered that the fluid's velocity magnitude decreases at the bottom wall and rises at the higher wall when it collides with the screen. Because of this, the higher walls exhibit the greatest pressure reduction. Tarafder and Mia [34] focused the range of velocity in the pipe's upstream and downstream parts, as well as the pressure distribution over the contracting portion, are presented in this study for Reynolds values of 372 and 968, correspondingly. This report compares the outcomes of experiments using Open-FOAM and COMSOL Multiphysics. Malikov et al. [14] studied the application of the Comsol Multiphysics applications and demonstrated the two-fluid turbulence algorithm's excellent precision, stability, and convergent. The objective of this research is to examine parameters that affect the fluid-particle interactions. Marin et al. [35] examined the velocity is impacted by changing the variables, two different types of velocity profile plots are shown: one parallel to the plates and the other orthogonal to the plates. To see the physical significance of COMSOL Multiphysics, MHD, heat transfer and viscous fluids; a list of core investigation relevant to the present study are given in [36-48].

In this paper, the flow of a Newtonian fluid flow through a two-dimensional cylinder with a contraction and a solid fragment is investigated. The effects of the contraction and the steel fragment on the fluid's velocity, pressure, temperature and convection of heat are examined. Section 2 contains formulation of the problem. Simulation and methodology are given in Section 3. The graphical discussion is given in Section 4. In last Section 5 key observations are listed.

2. Mathematical modelling

The study proposes a Newtonian incompressible fluid flowing through a 2D cylinder. The fluid is flowing through a cylinder with an airfoil shaped disturbance inside it. Figure 1 shows the geometry of the cylinder with airfoil fragment. The fluid flow is considered to be in x-axis and y-axis. The radius of the cylinder is 0.7m and the length of the cylinder be 2m with location x=0 and y=0. The compacted regions radius be 0.4m. The fragment inside the cylinder was made using polygon with coordinates x(0.35, 0.5, 0.6, 0.6, 0.35) and y(0.35, 0.45, 0.4, 0.3, 0.35). The fluid flow and heat transfer are introduced to COMSOL Multiphysics by using the add physics tool. Inlet and outlet of the flow are selected and the velocity of flow at the boundary were zero. The temperature at the boundary of the fragment is supposed to be 315K. The initial temperature is 273K. The temperature at upper and lower boundary are temperature (T1) and temperature (T2) with 298K and 300.5K respectively. The properties of the fluid and fragment properties inside a cylinder is addressed.

Continuity equation:

$$u_x + v_y = 0. \tag{1}$$

Momentum equation:

$$\left.\begin{aligned}\rho_{hnf}\left(u_t + uu_x + vu_y\right) &= -p_x + \partial_y\left(v_x - u_y\right)\mu_{hnf}\\ \rho_{hnf}\left(v_t + uv_x + vv_y\right) &= -p_x - \partial_x\left(v_x - u_y\right)\mu_{hnf}\end{aligned}\right\}. \tag{2}$$

Where the (ρ_{hnf}) is density of the hybrid nanofluid (μ_{hnf}) is viscosity of the nanofluid and (P) is pressure of the fluid.

Energy equation:

$$(\rho C_P)_{hnf}(\partial_t + v\partial_y + u\partial_x)T = k_{hnf}(\partial_{xx} + \partial_{yy})T. \quad (3)$$

The controlling heat transfer equation:

$$d_z(\rho C_p)\left(\frac{\partial T}{\partial t}\right) + d_z\rho C_p u.\nabla T + \nabla.q = d_z Q + q_0 + d_z Q_p + d_z Q_{vd}. \quad (4)$$

Heat transfer equation of the solid fragment inside the fluid:

$$d_z(\rho C_p)\left(\frac{\partial T}{\partial t}\right) + d_z\rho C_p u.\nabla T + \nabla.q = d_z Q + q_0 + d_z Q_{ted}, \quad (5)$$

$$q = -d_z k\nabla T. \quad (6)$$

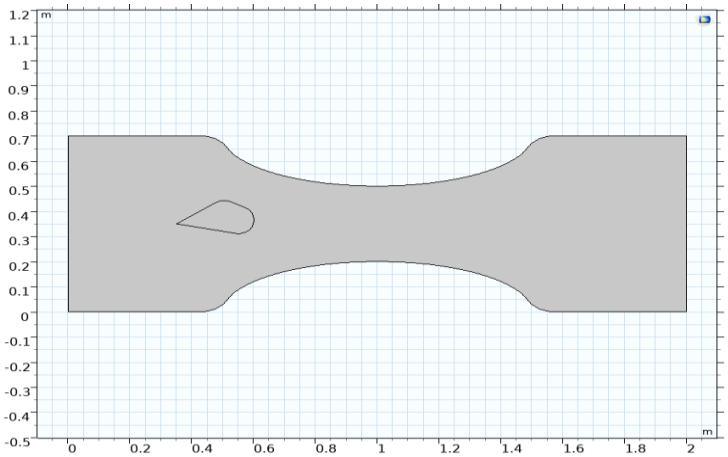

Fig.1: Geometry of the problem.

Where $Q_{vd} = \tau\nabla u$ denotes the viscous dissipation heat source $\tau = -PI + K, q = -d_z k\nabla T$ whereas Q denotes heat source ∇T denotes temperature gradient and d_z is the fluid's thickness.

Initial conditions:

The initial condition are supposed to be;

$$u = 0\ , v = 0, \quad T = T_0\ , and\ \ P = 0. \quad (7)$$

Thermophysical features of nanofluid:

The thermophysical relation of the hybrid nano particles are defined below;

$$\rho_{hnf} = (1 - \phi_2)\left[(1 - \phi_1)\rho_f + \phi_1\rho_{s1}\right] + \phi_2\rho_{s2}, \quad (8)$$

$$\mu_{hnf} = \frac{\mu_f}{(1-\phi_1)^{2.5}(1-\phi_2)^{2.5}}, \tag{9}$$

$$(\rho C_p)_{hnf} = (1-\phi_2)[(1-\phi_1(\rho C_p)_f + \phi_1(\rho C_p)_{s1}] + (\rho C_p)_{s2}\phi_2, \tag{10}$$

$$\frac{k_{hnf}}{k_f} = \frac{k_{s1}+2k_f-2\phi_1(k_f-k_{s1})}{k_{s1}+2k_f+\phi_1(k_f-k_{s1})} * \frac{k_{s2}+2k_f-2\phi_2(k_f-k_{s2})}{k_{s2}+2k_f+\phi_2(k_f-k_{s2})}. \tag{11}$$

Boundary conditions:

The boundary condition consists of inlet, outlet, at the surface of wall and thermal insulation.

The inlet

At 2D cylinder entrance, Newtonian fluid rate was estimated. The fluid volume can be adjusted by area of inflow path and velocity intake. Fig. 2 shows model's input. The inlet boundary conditions are as follows:

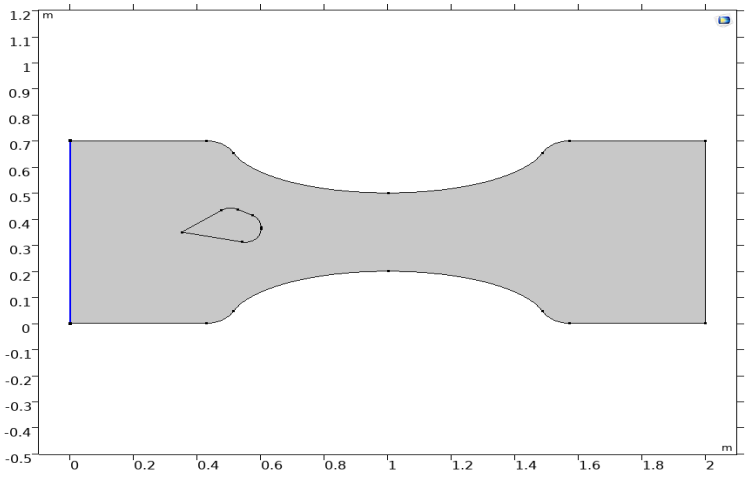

Fig. 2 Inlet boundary condition.

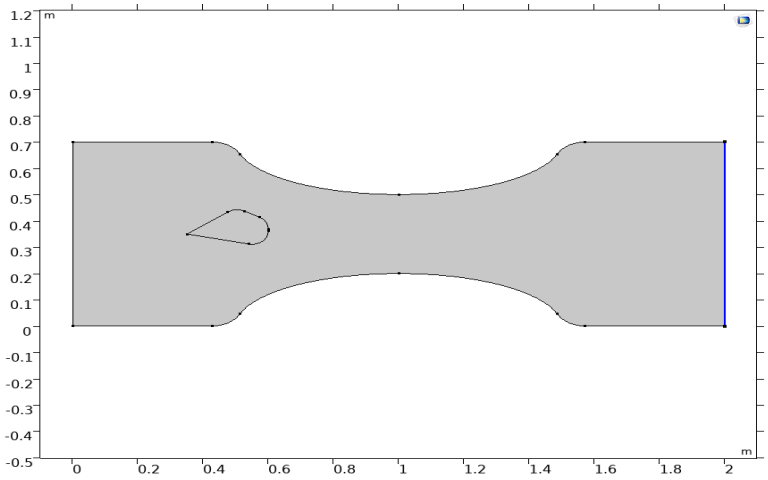

Fig. 3 Outlet boundary condition.

$$u(x, y, t) = -u_0 n\ . \tag{12}$$

The outlet:
To improve realism, pressure at the outflow is included to the model. Fig. 3 shows the outlet boundary condition.

$$[-pI + K]n = -p_0 n, \qquad \text{where} \quad p_0 \leq p. \tag{13}$$

At the wall:
The Newtonian fluid under examination sticks to the wall because to its viscosity and cannot flow through it. The no-slip condition and boundary conditions are then measured at the wall. Fig. 4 shows the walls of the 2D cylinder.

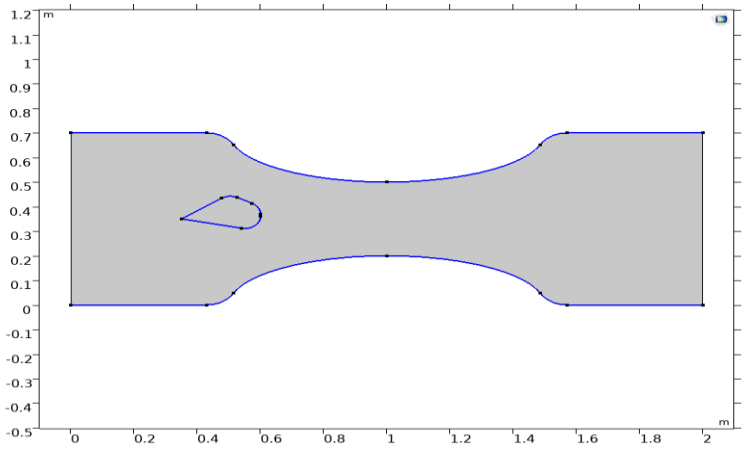

Fig. 4 Velocity at wall.

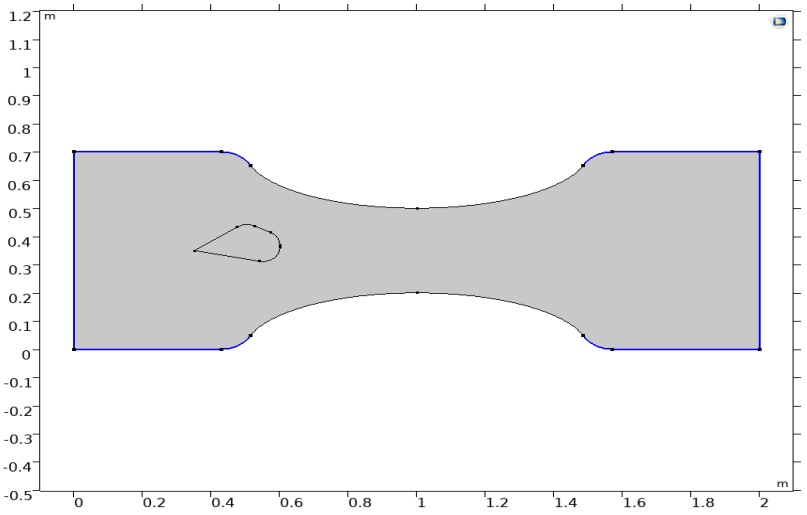

Fig. 5 Thermal insulation.

$$u = 0, \quad v = 0. \tag{14}$$

$$-n.q = 0. \tag{15}$$

Thermal insulation:
The insulating boundaries in COMSOL heat transfer module are shown in Fig. 5. Thermal insulation equation in COMSOL is defined as:

Temperature:
Temperature at upper and lower boundary in COMSOL Multiphysics are shown in Fig.6 and Fig. 7. The temperature at upper boundary is 298K and temperature at lower boundary is 300.5K.

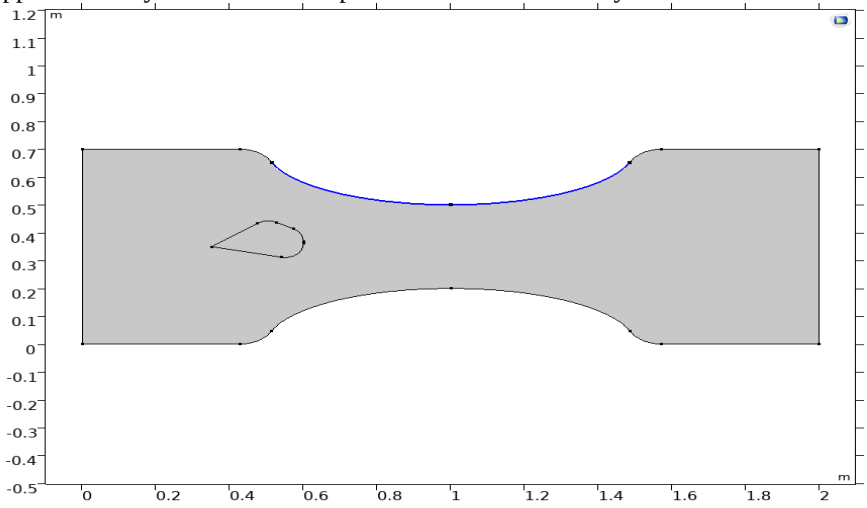

Fig. 6 Temperature at upper boundary.

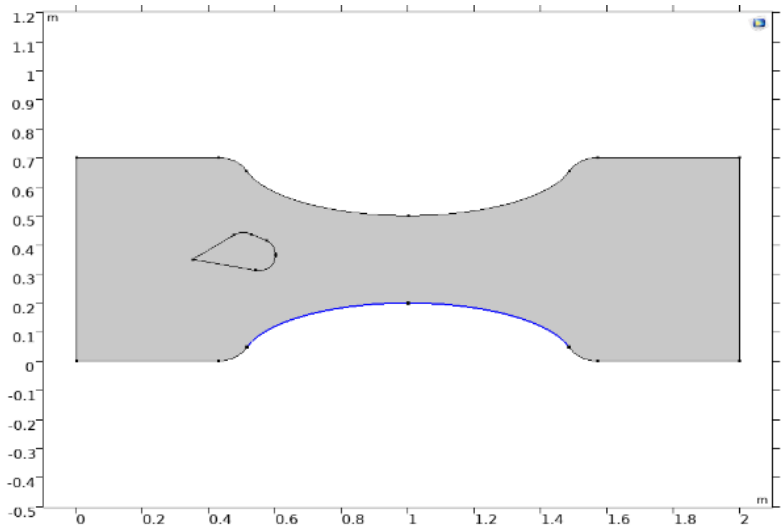

Fig. 7 Temperature at lower boundary.

Temperature at the surface of the solid fragment:
The temperature of solid fragment inside the pipe is set to be 315K which is shown in Fig.8.

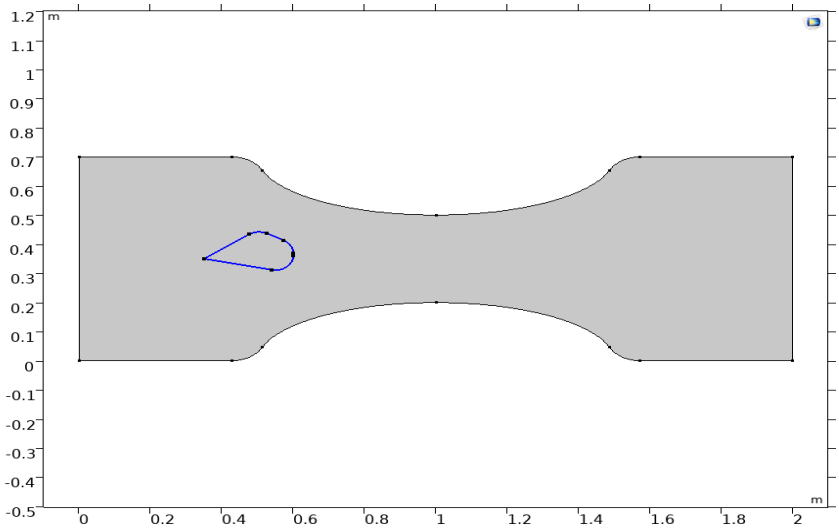

Fig. 8 Temperature of solid fragment inside the pipe.

Computational mesh:
A mesh is a necessary part of (Computational Fluid Dynamic) CFD. The mesh quality influences the solution's precision and its pace of convergence. The mesh is created using COMSOL's 'physics driven mesh'. Fig. 9 shows a fine size of element mesh.

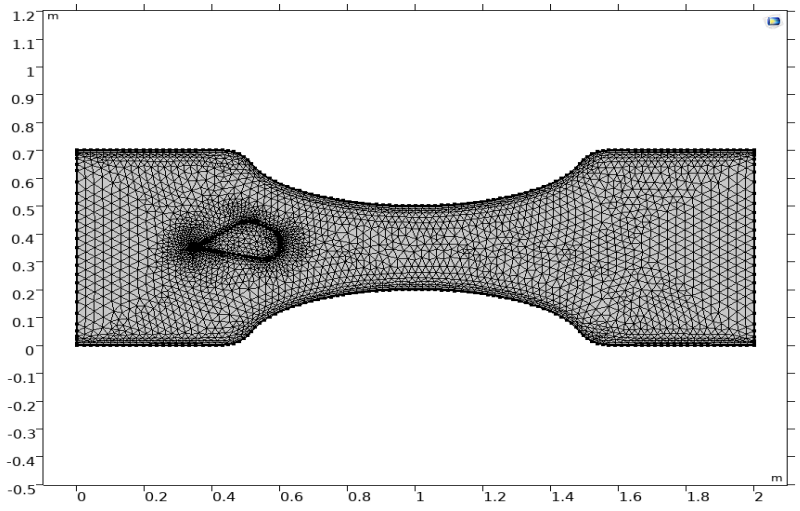

Fig. 9 Mesh size for considered geometry.

3. Discussion

The numerical simulation of hybrid nanofluid within a cylinder over an airfoil are addressed with an application of computation fluid dynamics tools i.e. COMSOL Multiphysics. The results of the contraction in

the cylinder with a solid fragment inside it are addressed in this section. The obtained results showed that one of the main factors causing high pressure at the walls of the pipe and disturbance in the flow of the fluid caused by contraction in the cylinder and presence of the solid fragment inside cylinder.

3.1 Surface velocity magnitude:

Fig. 10 (a,b,c,d) depicts the values of the surface velocity profile for intervals at 0.2 s, 0.8 s, 1.2 s, and 2 s.

Table 1: Physical properties of nanofluid and hybrid nanofluid.

Properties	Al_2O_3	Cu
$C_p(\frac{J}{KgK})$	765	385
$\rho(\frac{kg}{m^3})$	3970	8933
$k(\frac{W}{mK})$	40	400
Pr	-	-

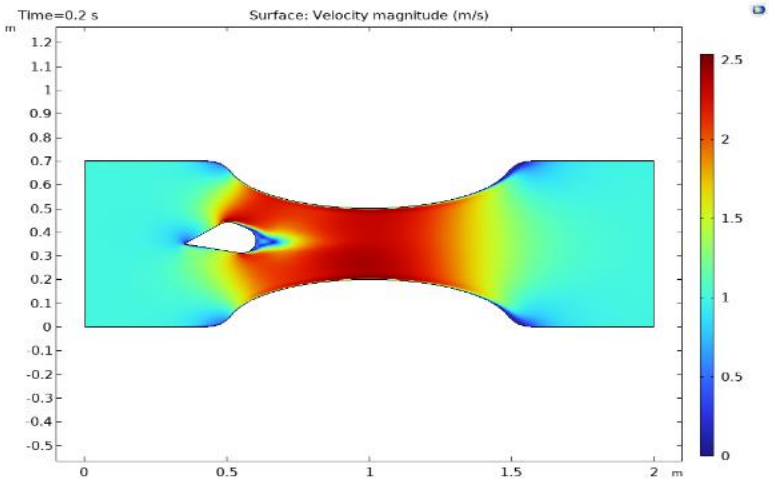

A. Velocity magnitude at 0.2s

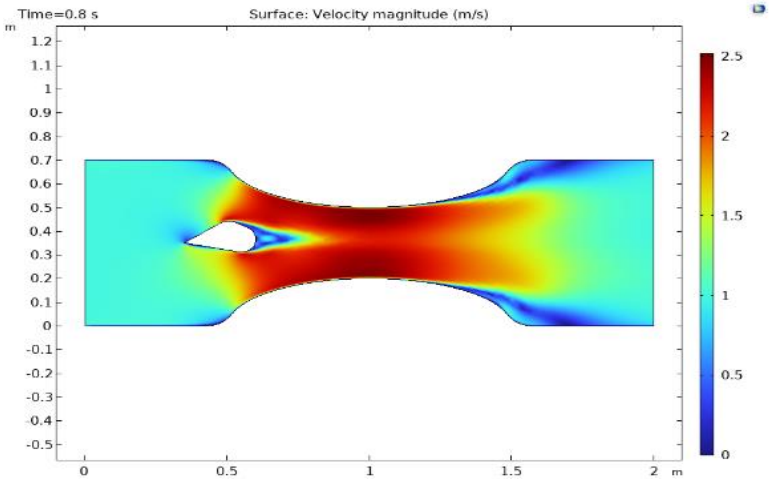

B. Velocity magnitude at 0.8s

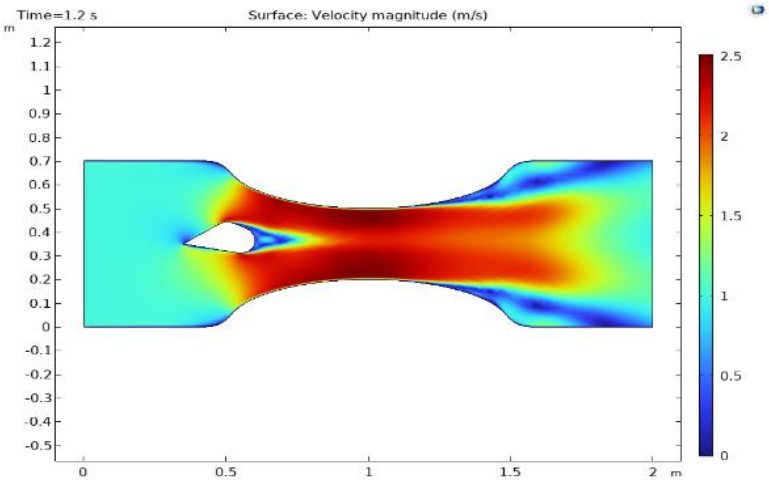

C. Velocity magnitude at 1.2s

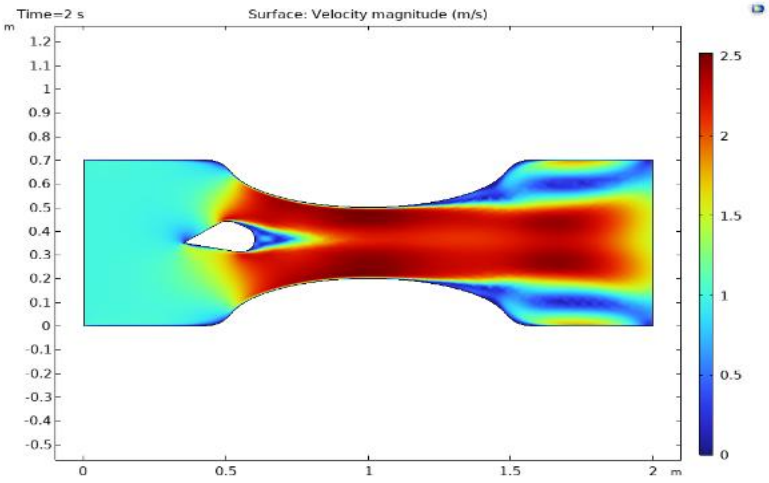

D. Velocity magnitude at 2s

Fig. 10 Surface velocity magnitude along the x-axis for different time step.

Fig. 10(a) shows initial stage of Newtonian hybrid nanofluid moving freely experiences contraction at a particular location in the cylinder, creating a sudden increase in velocity along a specific path due to presence of the solid fragment. The fluid's velocity changes when it comes in contact with the solid segment, causing the fluid to split above and below. The fluid's separation point is just above and below the fragment's walls; at this point, the velocity tends to zero. Where the peak velocity is around 2.50m/s at 0.2s in the centre of contracted cylinder. Fig. 10(b) shows the velocity at 0.8 seconds, noting that as the flow exits the contracted region, it starts to disperse, with the highest surface velocity around 0.6 m/s at the top and bottom edges of that connected cylinder. Fig. 10(c) at 1.2 seconds, shows a 0.01% increase in surface velocity compared to earlier times, with swirling motions observed when the nanofluid motion is highest. Finally, Fig. 10(d) indicates that as nanofluid pass the contracted area, flow circulation intensifies, increasing pressure on the cylinder walls. The highest surface velocity of 2.16m/s is seen at the centre, while lower velocities of 1.25m/s are observed just below the upper and above the lower cylinder walls.\

3.2 Velocity distribution for horizontal and vertical directions:

Fig. 11(a,b,c,d) displays the horizontal velocity profile (x-axis) at times 0.2s, 0.8s, 1.2s, and 2s.

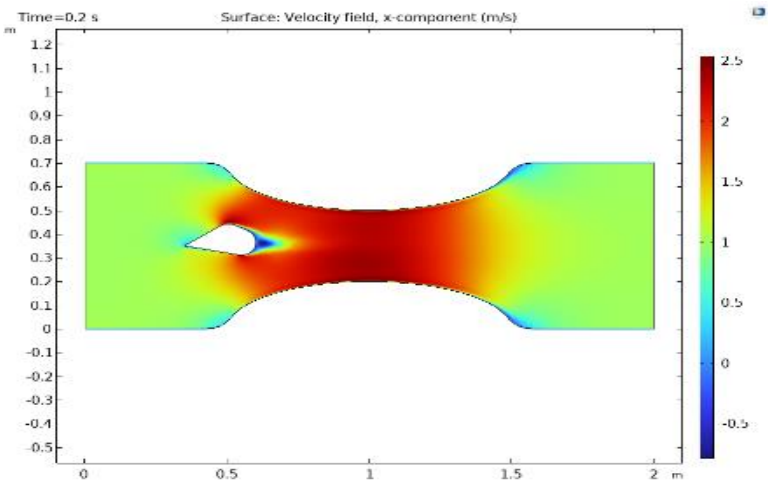

A. Velocity component in x-axis at 0.2s

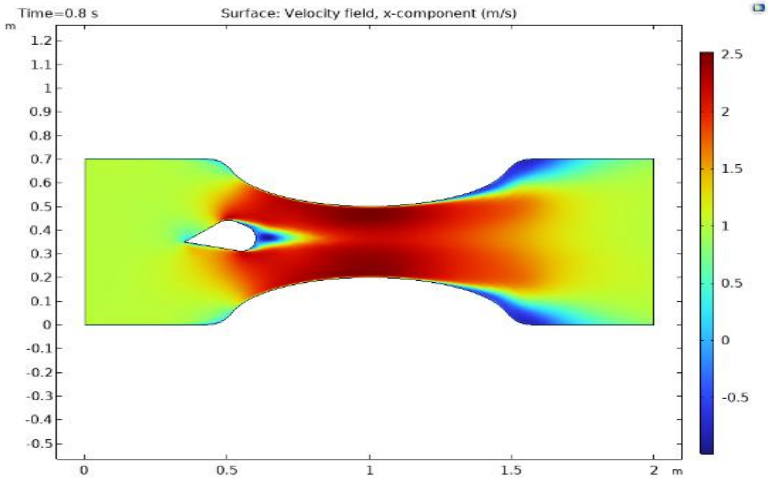

B. Velocity component in x-axis at 0.8s

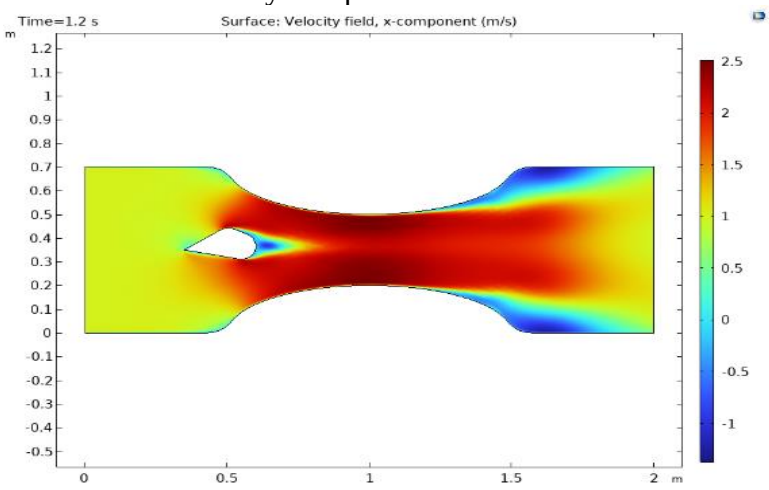

C. Velocity component in x-axis at 1.2s

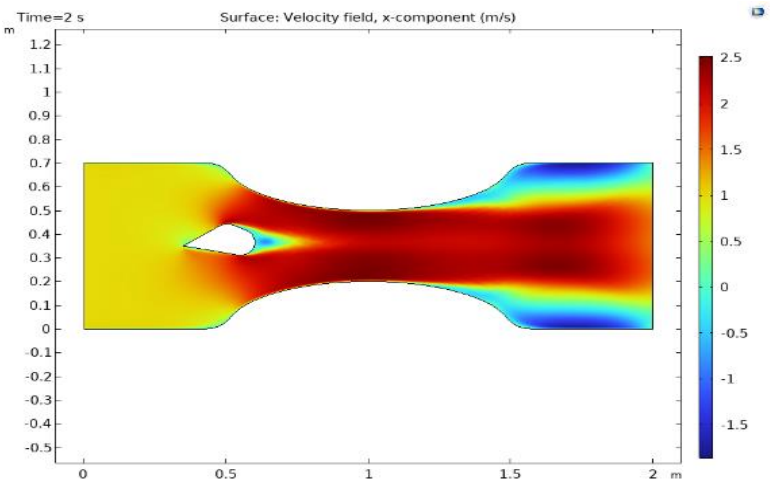

D. Velocity component in x-axis at 2s

Fig. 11 Surface velocity distribution profile at x-axis for different time.

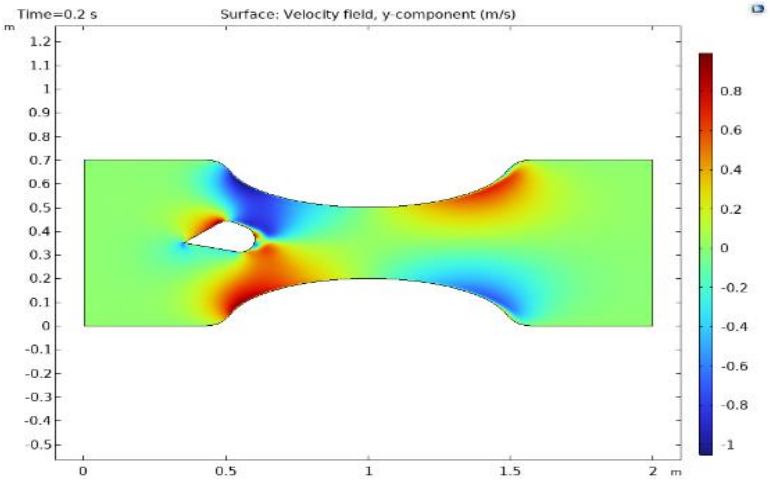

A. Velocity component in y-axis at 0.2s

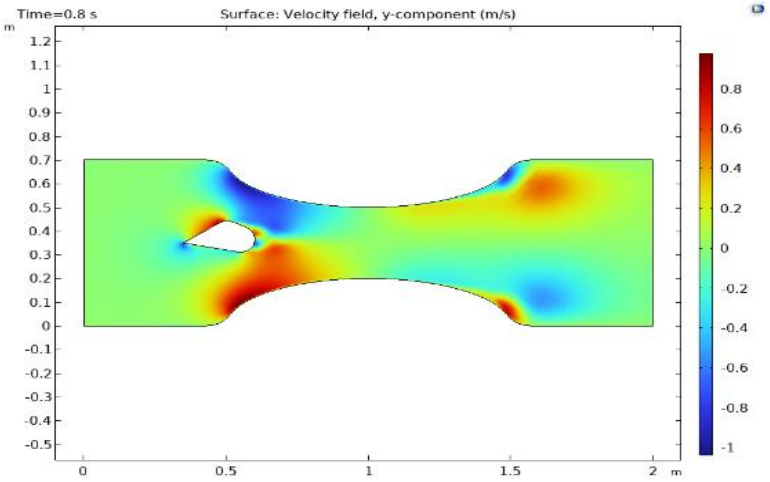

B. Velocity component in y-axis at 0.8s

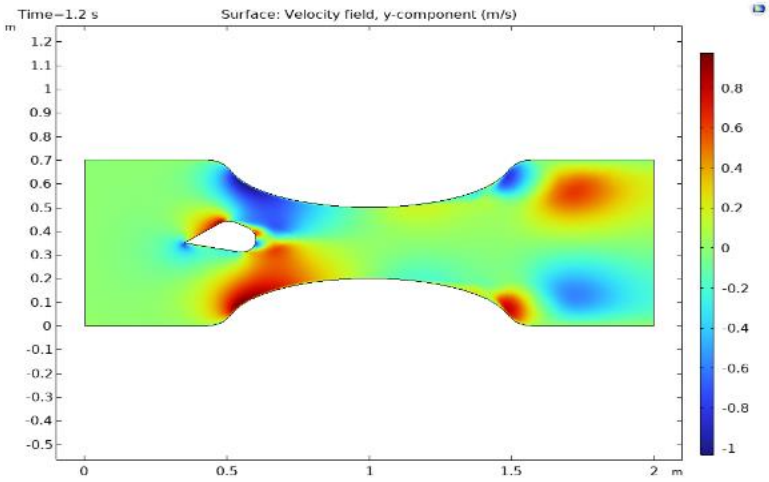

C. Velocity component in y-axis at 1.2s

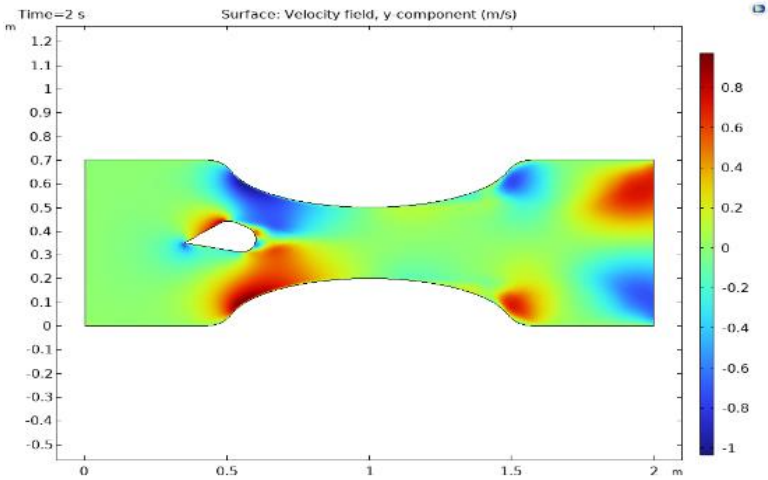

D. Velocity component at y-axis at 2s

Fig. 12 Velocity profile at y-axis.

The surface velocity profile along the vertical plane (y-axis) are shown on Fig. 12(a,b,c,d) at times 0.2s, 0.8s, 1.2s and 2s respectively.

The surface velocity reached an all-time high of 2.5m/s in its x-axis direction after 2 seconds. The confined area's minimum surface velocity is 2.1m/s at time 0.8s. It is important to note that the prior to and after contraction of the cylinder motion of a freely flowing Newtonian fluid is substantial. After passing through the narrowed region of the cylinder, the velocity suddenly increased, indicating that in the centre of flow configuration the pressure applied to the cylinder walls has increased because of the increased mobility of the nanofluid. As the contraction develops, this effect keeps getting better, and vice versa. Because of the presence of the solid fragment inside the cylinder it distributes the fluid above and below the fragment which effects velocity of fluid inside the cylinder. The effect of the contraction on velocity in the y-direction is displayed in Fig. 12(a,b,c,d). The surface velocity profile in the y-direction at time t=0.2 s is shown in Fig. 12(a). At 0.2 s, surface velocity along y-direction is measured to be 0.85 m/s interestingly, the surface velocity is minimum at the upper curved surface and largest at the lower starting point of the contracted area. Velocity profile along y-direction at 0.8 s is shown in Fig. 12(b), where the magnitude of the surface velocity has reduced. For, 0.8 s, the greatest surface magnitude is recorded at 0.8 m/s. The surface velocity magnitude at 1.2 s and 2 s,

respectively, is shown in Figs. 12(c,d). The surface velocity magnitude in Fig. 12(c) has increased to 0.8 m/s at 1.2 s, and it is seen that this rise continues as the time scale increases from 1.2s to 2s as shown in Fig. 12(c,d)respectively. Just above and below the solid fragment we can see a variation in velocity above the solid fragment the velocity higher and below its velocity is lower as compare to the upper part.

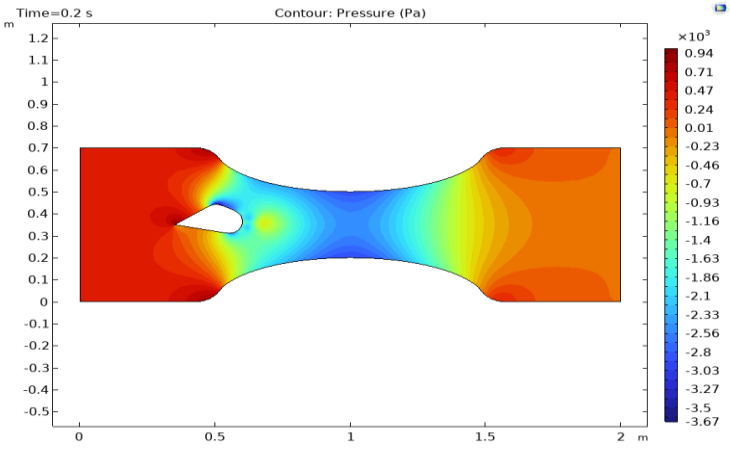

A. Pressure contour at 0.2s

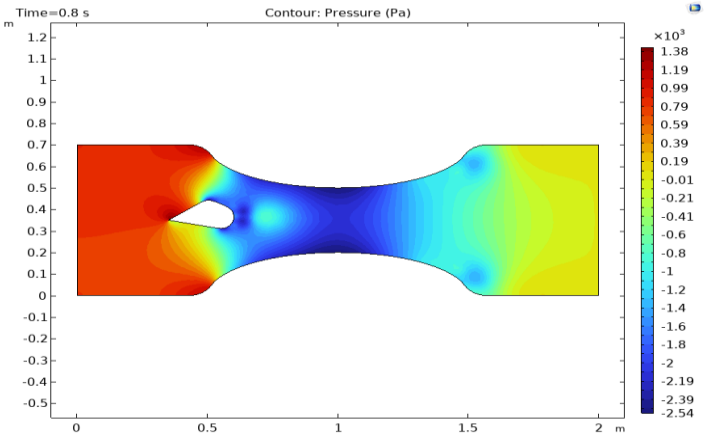

B. Pressure contour at 0.8s

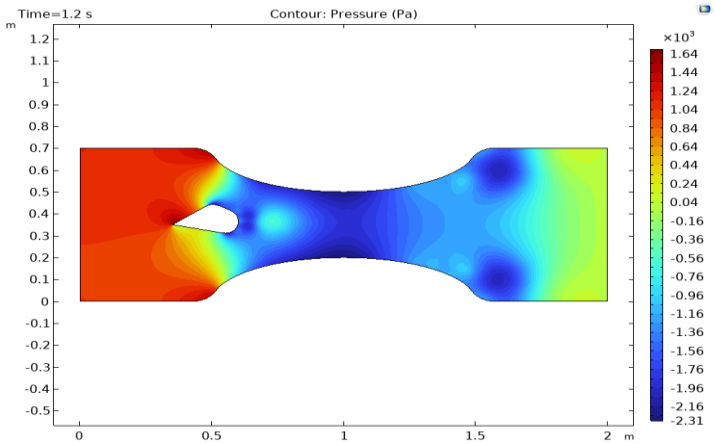

C. Pressure contour at 1.2s

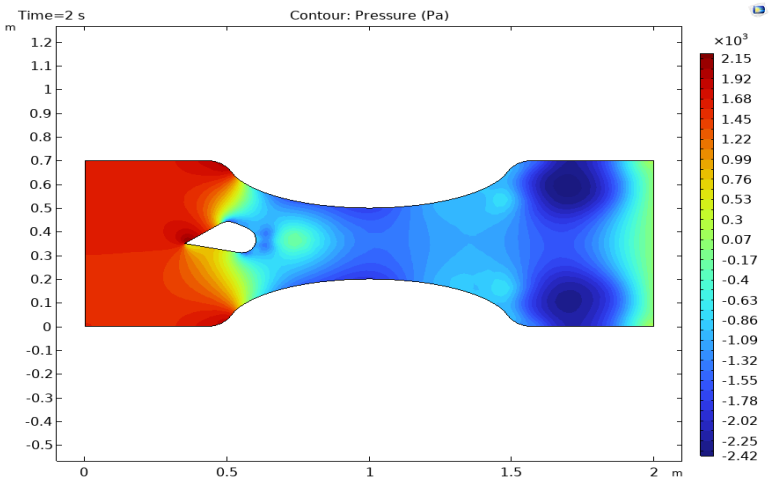

D. Pressure contour at 2s

Fig. 13 Surface pressure contour plot for time.

3.2 Pressure profile:

The applied pressure of Newtonian nanofluid flow via the contracted cylinder is depicted in Fig. 13(a,b,c,d) at various time scales: 0.2 s, 0.8 s, 1.2 s, and 2 s.

The pressure that a contracted cylinder experiences at its wall as a result of the motion of nanofluid is shown in Fig. 13(a). It can be seen that the pressure profile peaked at 0.94 Pa at the beginning of the contraction. Because of the presence of solid fragment after the separation at upper and lower boundary the velocity of the fluid decreases because of that the pressure at the area increases so at the back of the fragment values of pressure is -1.4 pa and 1.1pa respectively. It is important to note that minimal pressure was detected when the freely flowing fluid reaches the contracted configuration's centre. This implies that the Newtonian nanofluid is moving at its maximum speed in the contraction's centre, and as a result, there is very low pressure above and below the walls. At 0.8 s, the pressure profile is shown in Fig. 13(b). The pressure that is being applied has suddenly increased to 0.79 Pa, and centre of contracted area present a low-pressure profile. Fig. 13(c) shows that the pressure profile increased rapidly at time 1.2 s. This phenomenon of increased pressure profile is caused by increased fluids motion. The pressure profile at time scale 2 s boundary point is displayed in Fig. 13(d). Also, 2.15 Pa more pressure has been exerted, and the minimal pressure profile has dropped to -2.42 Pa. It is worth noting that the Newtonian nanofluid's swirling motion has increased near the outlet wall. Furthermore, it has been discovered that the region of the narrower cylinder is directly responsible for an increase in pressure.

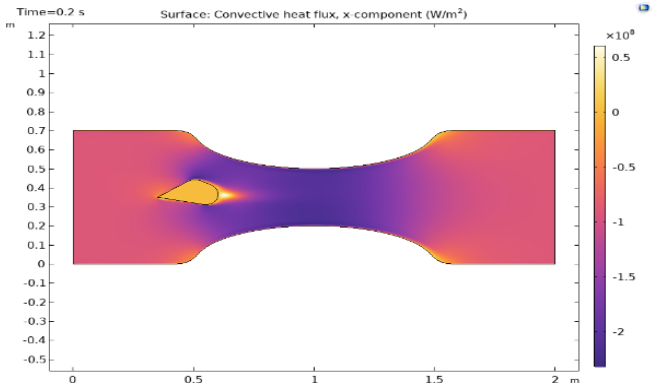

A. Heat flux in x-axis at 0.2s

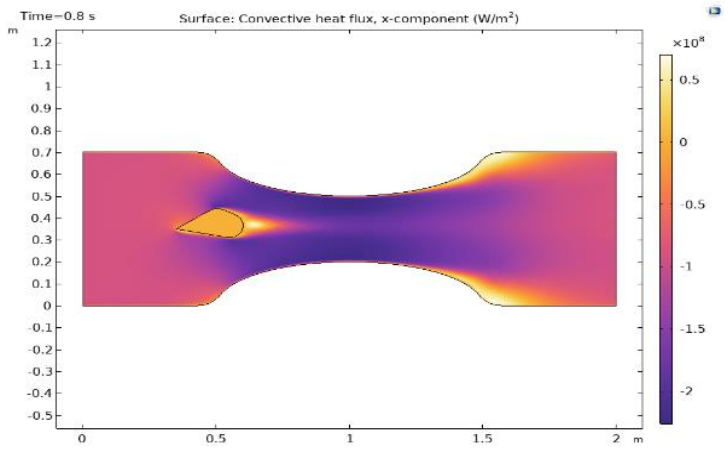

B. Heat flux in x-axis at 0.8s

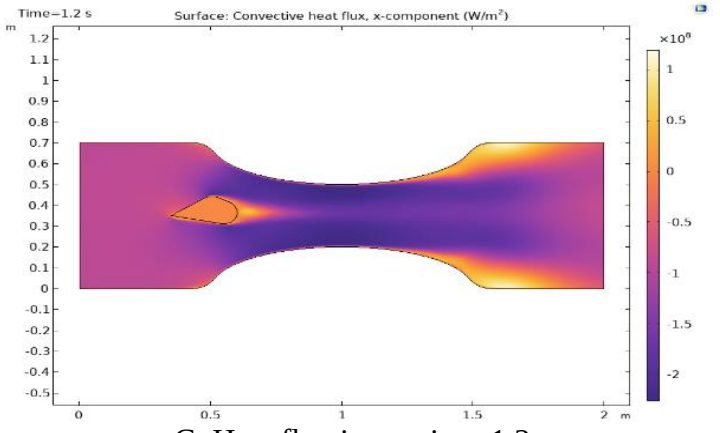

C. Heat flux in x-axis at 1.2s

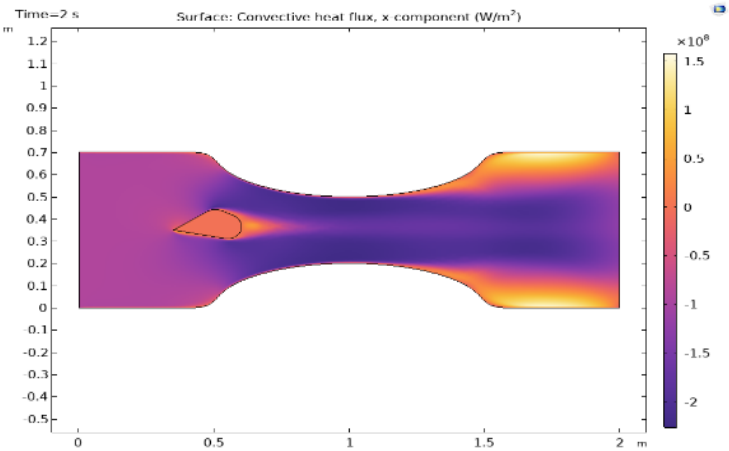

D. Heat flux in x-axis at 2s

Fig. 14 Surface contour plot of heat flux in x-direction for different time.

3.4 Convective heat flux:

The convective heat flux along the x-axis around a cylinder with an internal fragment at different times (0.2s, 0.8s, 1.2s, and 2s) is shown in Figure 14.

At 0.2 seconds (Figure 14a), the largest convective heat flux is observed at the boundaries of the supposed cavity, while the minimum heat flux is recorded in the contracted region of the pipe in the x-direction. At 0.8

seconds (Figure 14b), the area with the lowest heat flux in the x-direction due to convection has increased, with the minimum flux again observed at the artery wall. The convective heat flux profile at 1.2 seconds (Figure 14c) shows that the smallest region for convective heat flow in the x-direction has grown due to increased movement of the Newtonian nanofluid. The largest convection phenomena occur at the upper and lower walls of the configuration and the surface of the solid fragment, which has a slightly higher temperature than the upper and lower boundaries. At 2 seconds (Figure 14d), the convective heat flux profile shows an increased nanofluid velocity in the configuration's center, with the maximum heat flux in the x-direction reaching 1.5E8. The heat flux approaches its maximum of 1.5E8 and its minimum of -2E8 at this time. At the fragment boundary where separation occurs and on the back side, the heat flux is 3.1E7 at 2 seconds.

Fig. 15 (a,b,c,d) depicts the convective heat flux along the y direction at intervals of 0.2 s, 0.8 s, 1.2 s, and 2 s. It is worth noting that the patterns of the convective heat flux profile and the surface velocity magnitude profile across the y-direction are identical, implying that convection along the y-direction requires Newtonian fluid motion. In the constricted cylinder with an internal fragment, higher starting and lower ending positions are observed (Figure 15a). The maximum convective heat flux at 0.2 seconds is 8.003E7. At 0.8 seconds (Figure 15b), despite an increase in the area covered by the convective flow profile, the heat flux from convection progresses further along the area. The convective heat flux in the y-direction at 1.2 seconds (Figure 15c) decreases with the addition of nanofluid. At 2 seconds (Figure 15d), a dispersed convective heat flux is observed in the y-direction, with the highest heat flux measured at 9.25E7. The heat flux profile decreases in the y-direction due to minimal motion of the blood-based nanofluid. The convective heat flux patterns in both the x and y-directions indicate that the narrow region has the lowest heat flux, although smoother motion results in higher heat flux profiles for nanofluids.

3.5 Surface temperature:

The surface temperature of the flow is shown in Fig. 16(a,b,c,d) at 0.2s, 0.8s, 1.2s and 2s respectively.

The contracted pipe's higher and lower boundaries, with the solid fragment inside, had the highest surface temperature. The temperature between upper and lower boundaries ranges from 270K to 285 K. Fig. 16(a,b,c,d) shows that the ambient temperature of the pipe's upper and lower borders, as well as the surface of the solid fragment, increases over time. The temperature on the surface of a solid fragment reaches a maximum of 315K. The temperature at the upper and bottom boundaries of the 2D pipe was 298K and 300.5K, respectively.

3.6 Temperature contour:

Fig. 17(a,b,c,d) shows temperature contours at 0.2, 0.8, 1.2, and 2 s.

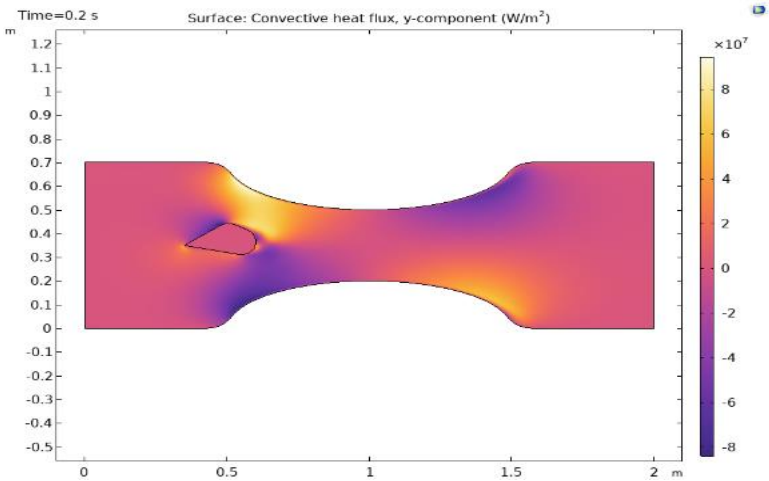

A. Heat flux in y-axis at 0.2s

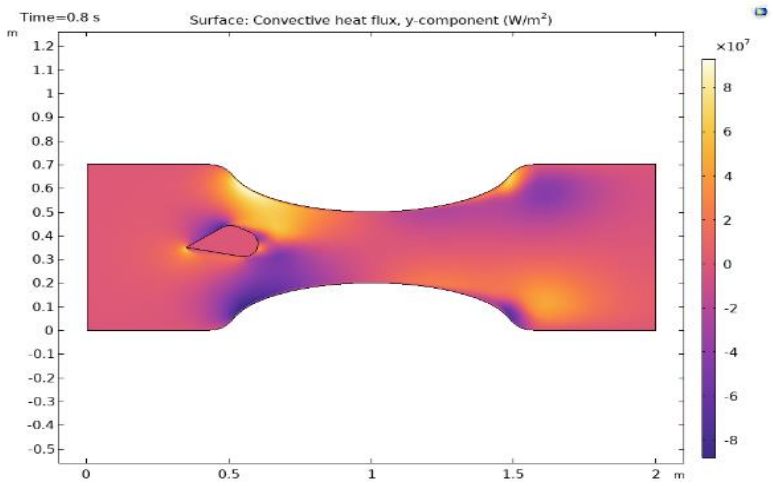

B. Heat flux at y-axis at 0.8s

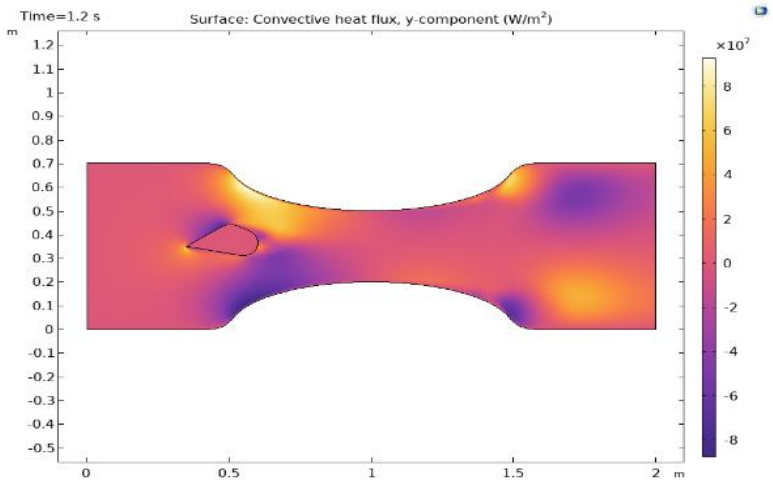

C. Heat flux at y-axis at 1.2s

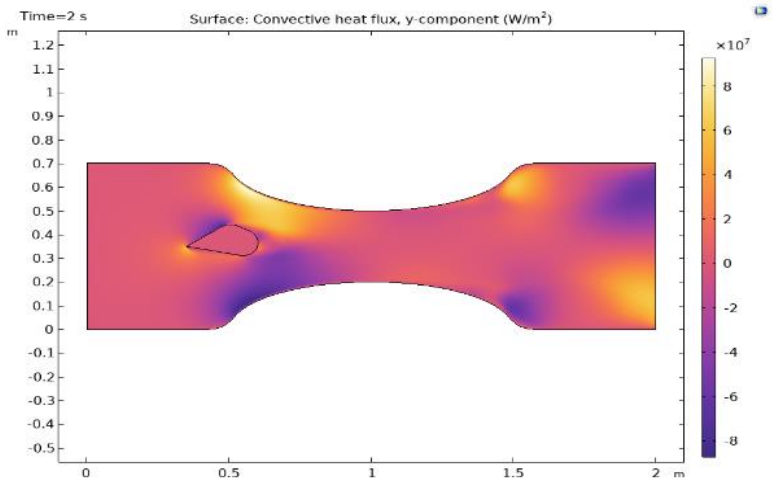

D. Heat flux at y-axis at 2s

Fig. 15 Surface contour plot of heat flux in y-direction for different time.

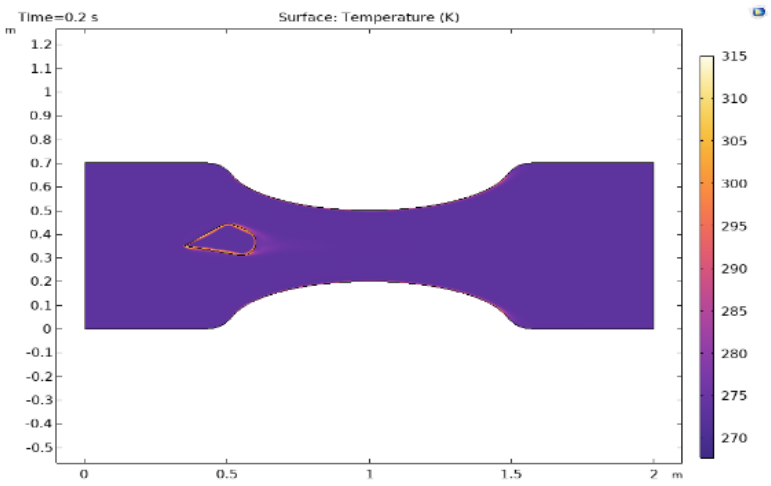

A. Surface temperature at 0.2s

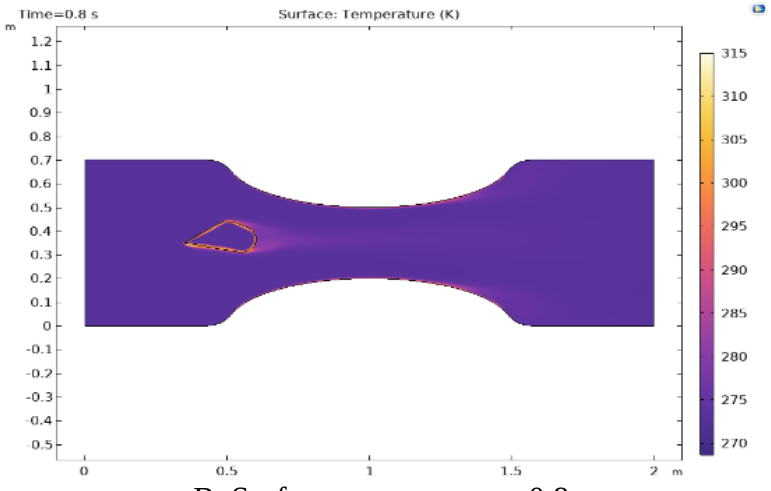

B. Surface temperature at 0.8s

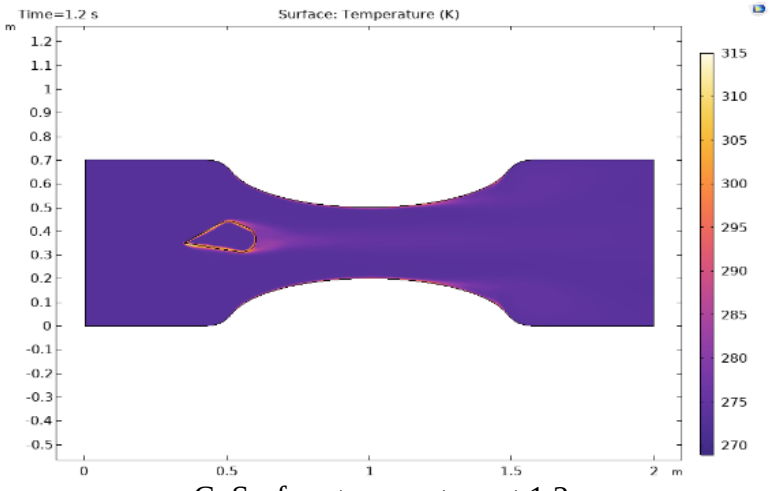

C. Surface temperature at 1.2s

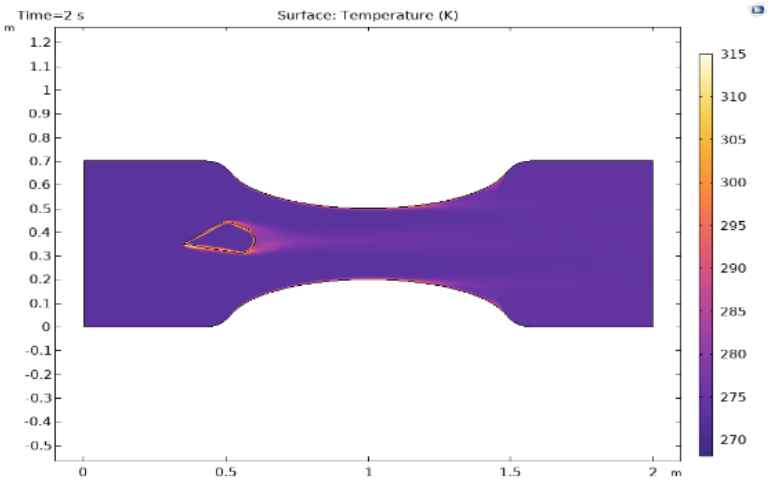

D. Surface temperature at 2s

Fig. 16 Surface plot of temperature distribution for different time.

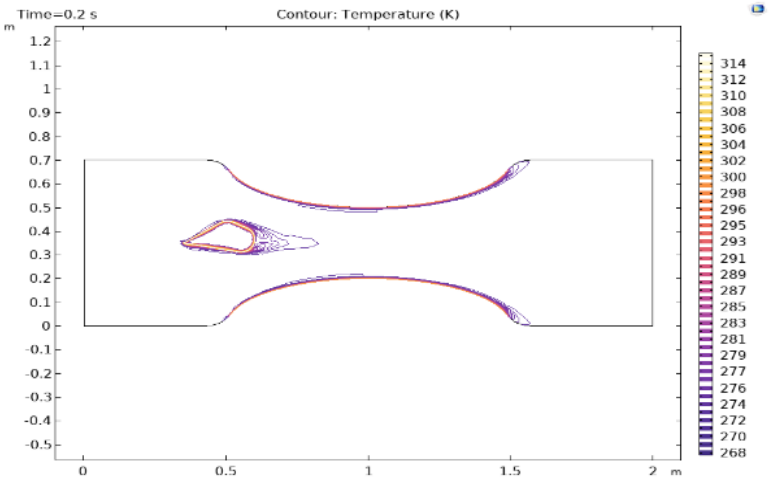

A. Temperature contour at 0.2s

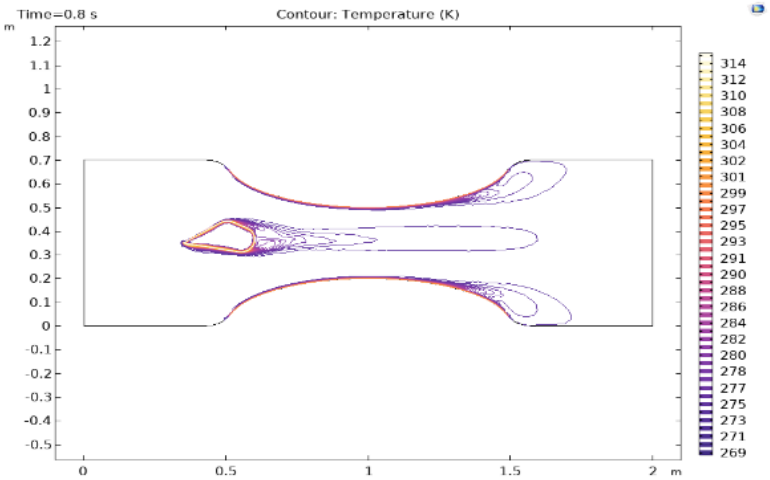

B. Temperature contour at 0.8s

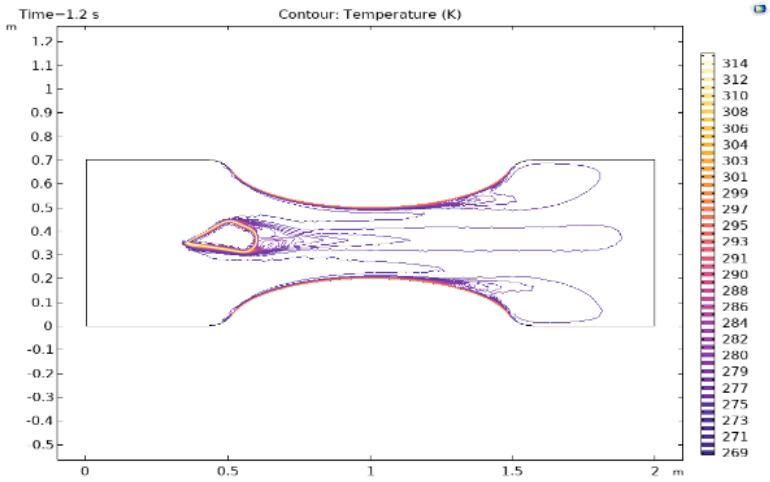

C. Temperature contour at 1.2s

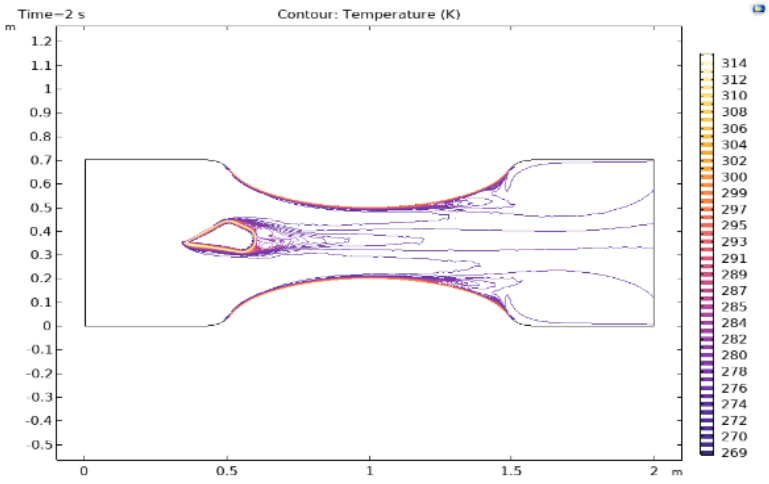

D. Temperature contour at 2s

Fig. 17 Temperature contour plot along x-axis for different time.

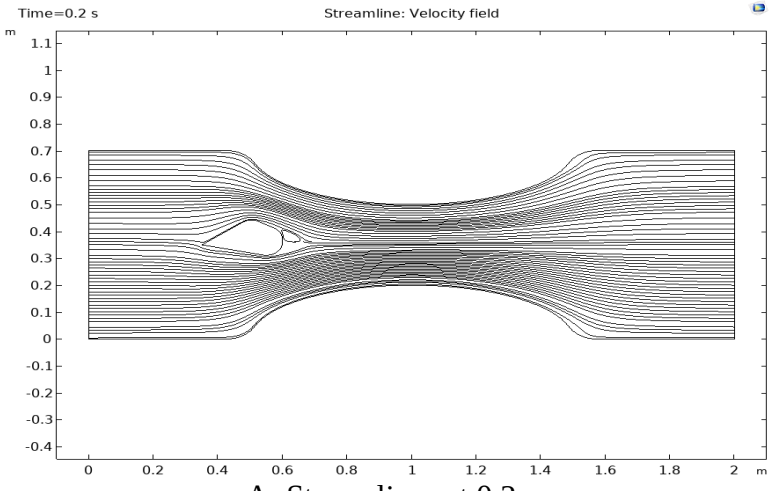

A. Streamlines at 0.2s

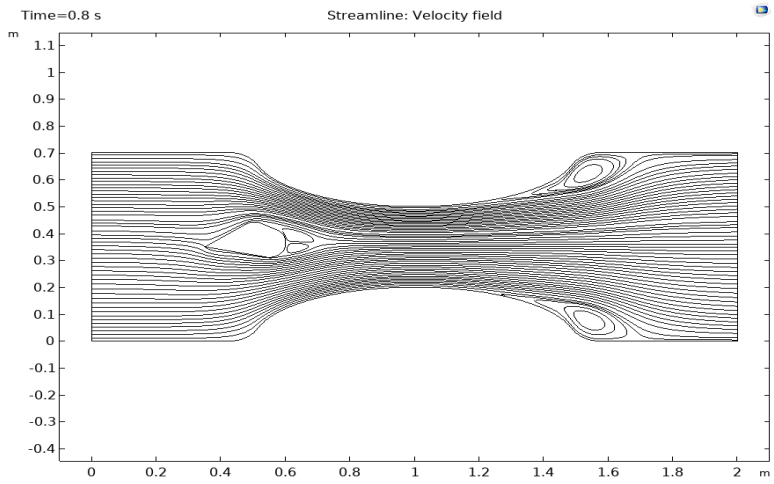

B. Streamlines at 0.8s

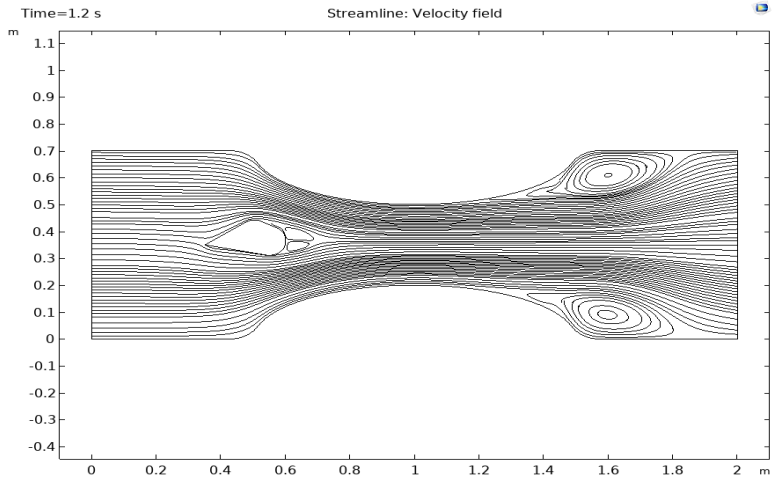

C. Streamlines at 1.2s

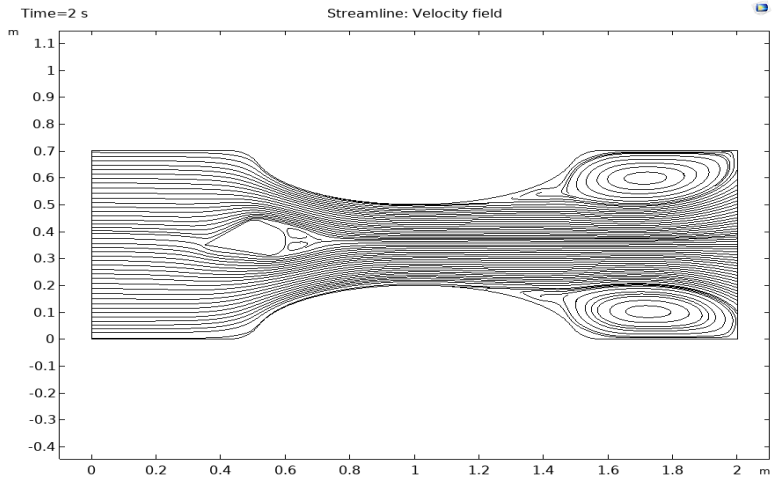

D. Streamlines at 2s

Fig. 18 Streamlines plot for x-axis flow direction for different time.

At 0.2 s, there are the fewest isothermal contours, while at 2 s, there are the most. As time passes, the velocity

of the nanofluid rises, resulting in larger thermal contours.

3.7 Streamline:

Fig.18 (a,b,c,d) show the streamlines for the current problem at 0.2s, 0.8s, 1.2s and 2s respectively.

Streamlines are predetermined lines that correspond to the motion of a free-flowing fluid at any particular time. Fig. 18(a) depicts the streamlines at time 0.2 seconds. Smooth flow patterns in streamlines are discovered, but when they came into touch with the solid component placed inside the fluid, a disturbance in the streamlines was seen. At 0.8 s, Fig. 18(b) shows how the Newtonian nanofluid slightly starts to disperses the streamline pattern as it passes through the contracted area and at the solid fragments separation points. Fig. 18(c) shows the streamlines pattern at 1.2 seconds. The whirling motion observed in the surface velocity magnitude profile is also visible in the streamline profile following contraction. Fig. 18(d) depicts streamlines at 2 seconds. The swirling motion accelerates toward the curved portion of the cylinder's contracted section. Furthermore, the streamline path is disturbed by the rapid motion of Nano-fluid in the contract area of the cylinder after it comes into contact with the solid fragment. A wake can be seen behind the solid fragment that disrupt the flow of the fluid at the region.

4. Conclusion

The numerical simulation of boundary layer flow of Newtonian hybrid nanofluid within cylinder is analysed. The hybrid nanoparticles used are aluminium oxide and copper. The computational fluid dynamics tool i.e. COMSOL Multiphysics is applied for the numerical simulation of boundary layer flow of hybrid nanofluid within a cylinder over an airfoil. COMSOL Multiphysics is powerful simulation is applied in this analysis that is based on finite element technique. The following important findings are addressed below:

- The nanoparticles inside the Newtonian fluid increases the fluid's flow performance.
- The highest velocity at contracted area 2.5m/s is observed whereas solid fragment inside a cylinder causes a disruption in fluid flow creating wake behind it.
- At different time spans temperature contour can be seen that shows increase in temperature contour as time grows.
- The streamline shows unusual behaviour at the contracted region of the cylinder showing incensement in streamline at that region and after involvement of the solid fragment the disruption in the streamline can be seen in front and behind the fragment.
- The temperature of the fluid changes after getting in contact with the wall of the cylinder and the solid fragment.
- The pressure at the contracted area and near the solid fragment shows unique features. The pressure increases as the time goes by at the inlet of the cylinder and decreases at the outlet and behind the solid fragment because of separation the pressure increases.

Reference

[1] S. U. S. Choi, J. Eastman, 1995, *Enhancing thermal conductivity of fluids with nanoparticles*,

[2] J. Akram, N. Akbar, D. Tripathi, Analysis of Electroosmotic Flow of Silver-Water Nanofluid Regulated by Peristalsis Using Two Different Approaches for Nanofluid, *Journal of Computational Science*, Vol. 62, pp. 101696, 05/01, 2022.

[3] S. Z. Alamri, R. Ellahi, N. Shehzad, A. Zeeshan, Convective radiative plane Poiseuille flow of nanofluid through porous medium with slip: An application of Stefan blowing, *Journal of Molecular Liquids*, Vol. 273, pp. 292-304, 2019/01/01/, 2019.

[4] F. Selimefendigil, H. Öztop, M. Doranehgard, N. Karimi, Phase change dynamics in a cylinder containing hybrid nanofluid and phase change material subjected to a rotating inner disk, *The Journal of Energy Storage*, Vol. 42, pp. 103007, 10/01, 2021.

[5] P. Gholamalipour, M. Siavashi, M. H. Doranehgard, Eccentricity effects of heat source inside a porous annulus on the natural convection heat transfer and entropy generation of Cu-water nanofluid, *International Communications in Heat and Mass Transfer*, Vol. 109, pp. 104367, 2019/12/01/, 2019.

[6] A. Zeeshan, R. Ellahi, M. A. Rafique, S. M. Sait, N. Shehzad, Parametric Optimization of Entropy Generation in Hybrid Nanofluid in Contracting/Expanding Channel by Means of Analysis of Variance and Response Surface Methodology, *Inventions*, Vol. 9, No. 5, pp. 92, 2024.

[7] F. Selimefendigil, H. Öztop, A. Chamkha, MHD mixed convection of nanofluid in a cubic cavity with a conductive partition for various nanoparticle shapes, *International Journal of Numerical Methods for Heat & Fluid Flow*, Vol. 29, 04/09, 2019.

[8] M. Hassan, M. I. Marin, R. Ellahi, S. Z. Alamri, EXPLORATION OF CONVECTIVE HEAT TRANSFER AND FLOW CHARACTERISTICS SYNTHESIS BY Cu–Ag/WATER HYBRID-NANOFLUIDS, *Heat Transfer Research*, Vol. 49, pp. 1837-1848, 2018.

[9] M. Bhatti, A. As, T. Abbas, S. Alamri, R. Ellahi, Study of Activation Energy on the Movement of Gyrotactic Microorganism in a Magnetized Nanofluids Past a Porous Plate, *Processes*, Vol. 8, pp. 328, 03/11, 2020.

[10] R. Abo-Elkhair, M. M. Bhatti, K. Mekheimer, Magnetic force effects on peristaltic transport of hybrid bio-nanofluid (Au Cu nanoparticles) with moderate Reynolds number: An expanding horizon, *International Communications in Heat and Mass Transfer*, Vol. 123, pp. 105228, 04/01, 2021.

[11] A. Zeeshan, N. Khalid, R. Ellahi, M. Khan, S. Z. Alamri, Analysis of nonlinear complex heat transfer MHD flow of Jeffrey nanofluid over an exponentially stretching sheet via three phase artificial intelligence and Machine Learning techniques, *Chaos, Solitons & Fractals*, Vol. 189, pp. 115600, 2024.

[12] R. Ellahi, The effects of MHD and temperature dependent viscosity on the flow of non-Newtonian nanofluid in a pipe: Analytical solutions, *Applied Mathematical Modelling*, Vol. 37, No. 3, pp. 1451-1467, 2013/02/01/, 2013.

[13] M. Turgay, A. Yazıcıoğlu, Numerical simulation of fluid flow and heat transfer in a trapezoidal microchannel with COMSOL multiphysics: A case study, *Numerical Heat Transfer, Part A: Applications*, Vol. 73, pp. 1-15, 02/22, 2018.

[14] Z. Malikov, M. Madaliev, S. Chernyshev, A. Ionov, Validation of a two-fluid turbulence model in comsol multiphysics for the problem of flow around aerodynamic profiles, *Scientific Reports*, Vol. 14, 01/27, 2024.

[15] S.-R. Yan, D. Toghraie, L. Abdulkareem, A. a. Alizadeh, P. Barnoon, M. Afrand, The rheological behavior of MWCNTs–ZnO/Water–Ethylene glycol hybrid non-Newtonian nanofluid by using of an experimental investigation, *Journal of Materials Research and Technology*, Vol. 9, pp. 8401-8406, 07/01, 2020.

[16] U. S. Mahabaleshwar, G. P. Vanitha, L. M. Pérez, O. Manca, An MHD flow of non-Newtonian fluids with CNTs and heat transfer across a linearly shrinking sheet with slip and Biot number, *Journal of Magnetism and Magnetic Materials*, Vol. 577, pp. 170764, 2023/07/01/, 2023.

[17] H. Chahregh, S. Dinarvand, TiO 2 -Ag/blood hybrid nanofluid flow through an artery with applications of drug delivery and blood circulation in the respiratory system, *International Journal of Numerical Methods for Heat & Fluid Flow*, Vol. ahead-of-print, 03/02, 2020.

[18] I. Shahzadi, S. Bilal, A significant role of permeability on blood flow for hybrid nanofluid through bifurcated stenosed artery: Drug delivery application, *Computer Methods and Programs in Biomedicine*, Vol. 187, pp. 105248, 2020/04/01/, 2020.

[19] H. Basha, K. Rajagopal, N. Ahammad, S. Ss, S. Gunakala, Finite Difference Computation of Au-Cu/Magneto-Bio-Hybrid Nanofluid Flow in an Inclined Uneven Stenosis Artery, *Complexity*, Vol. 2022, pp. 1-18, 04/12, 2022.

[20] A. Ali, F. Mebarek-Oudina, A. Barman, S. Das, A. Ismail, Peristaltic transportation of hybrid nano-blood through a ciliated micro-vessel subject to heat source and Lorentz force, *Journal of Thermal Analysis and Calorimetry*, 05/29, 2023.

[21] A. Elelamy, N. Elgazery, R. Ellahi, Blood flow of MHD non-Newtonian nanofluid with heat transfer and slip effects: Application of bacterial growth in heart valve, *International Journal of Numerical Methods for Heat & Fluid Flow*, Vol. ahead-of-print, 03/05, 2020.

[22] A. Riaz, E. Bobescu, K. Ramesh, R. Ellahi, Entropy Analysis for Cilia-Generated Motion of Cu-Blood Flow of Nanofluid in an Annulus, *Symmetry*, Vol. 13, No. 12, pp. 2358, 2021.

[23] H. Waqas, U. Farooq, T. Muhammad, U. Manzoor, Importance of shape factor in Sisko nanofluid flow considering gold nanoparticles, *Alexandria Engineering Journal*, Vol. 61, No. 5, pp. 3665-3672, 2022/05/01/, 2022.

[24] T. Elnaqeeb, N. A. Shah, K. Mekheimer, Hemodynamic Characteristics of Gold Nanoparticle Blood Flow Through a Tapered Stenosed Vessel with Variable Nanofluid Viscosity, *BioNanoScience,* Vol. 9, 06/01, 2019.

[25] U. Khan, A. Zaib, A. Ishak, Magnetic Field Effect on Sisko Fluid Flow Containing Gold Nanoparticles through a Porous Curved Surface in the Presence of Radiation and Partial Slip, *Mathematics*, 04/21, 2021.

[26] D. Salvi, D. Boldor, G. M. Aita, C. M. Sabliov, COMSOL Multiphysics model for continuous flow microwave heating of liquids, *Journal of Food Engineering,* Vol. 104, No. 3, pp. 422-429, 2011/06/01/, 2011.

[27] B. Sezgin, G. Dilara, Caglayan, Y. Devrim, T. Steenberg, I. Eroglu, Modeling and sensitivity analysis of high temperature PEM fuel cells by using Comsol Multiphysics, *International Journal of Hydrogen Energy,* Vol. 41, 04/19, 2016.

[28] T. Adam, U. Hashim, COMSOL Multiphysics Simulation in Biomedical Engineering, *Advanced Materials Research,* Vol. 832, pp. 511-516, 11/01, 2013.

[29] M. Maliki, N. Laredj, K. Bendani, H. Missoum, Two-Dimensional Transient Modeling of Energy and Mass Transfer in Porous Building Components using COMSOL Multiphysics, *Journal of Applied Fluid Mechanics,* Vol. 10, pp. 319-328, 01/01, 2017.

[30] S. Salem, V. Tuchin, Numerical Simulation of Blood Flow in a Vessel by Using COMSOL Multiphysics® Software, *Annual Research & Review in Biology*, pp. 76-82, 09/02, 2020.

[31] W. Wijayanti, Musyaroh, M. N. Sasongko, R. Kusumastuti, Sasmoko, Modelling analysis of pyrolysis process with thermal effects by using Comsol Multiphysics, *Case Studies in Thermal Engineering,* Vol. 28, pp. 101625, 2021/12/01/, 2021.

[32] A. Hussain, A. Hassan, Q. A. Mdallal, H. Ahmad, E. M. Sherif, A. Rehman, M. Arshad, Comsolic solution of an elliptic cylindrical compressible fluid flow, *Sci Rep,* Vol. 11, No. 1, pp. 20030, Oct 8, 2021. eng

[33] A. Ganie, A. Ali, M. Memon, A. Albugami, K. Bhatti, I. Khan, Numerical analysis of laminar flow and heat transfer through a rectangular channel containing perforated plate at different angles, *Energy Reports,* Vol. 8, pp. 539-550, 12/20, 2021.

[34] S. Tarafder, M. Mia, 2022, *Comparative Numerical Simulation of Laminar Flow Through Pipe Using COMSOL Multiphysics and OpenFOAM*,

[35] J. C. Marín B., C. J. Amaya C., O. M. Ayala H., O. F. Ayala, M. Ayala, Numerical Study of the Velocity Profiles in an Incompressible Laminar Flow With Particles Between Two Parallel Plates, in *Proceeding of,* V009T10A051.

[36] A. Ali, M. Memon, K. Bhatti, K. Jacob, T. Sitthiwirattham, C. Promsakon, I. Khan, Modelling and Simulation of Fluid Flow through a Circular Cylinder with High Reynolds Number: A COMSOL Multiphysics Study, *Journal of Mathematics,* Vol. 2022, pp. 1-9, 05/19, 2022.

[37] G. Fatima, A. A. Khan, R. Ellahi, S. M. Sait, On hydromagnetic two-phase gas-liquid flow in ciliary channel: An application of a metachronal rhythm, *Chinese Journal of Physics,* Vol. 92, pp. 1435-1446, 2024/12/01/, 2024.

[38] I. K. Iliev, A. R. Gizzatullin, A. A. Filimonova, N. D. Chichirova, I. H. Beloev, Numerical Simulation of Processes in an Electrochemical Cell Using COMSOL Multiphysics, *Energies,* Vol. 16, No. 21, pp. 7265, 2023.

[39] S. Z. Alamri, A. A. Khan, M. Azeez, R. Ellahi, Effects of mass transfer on MHD second grade fluid towards stretching cylinder: A novel perspective of Cattaneo–Christov heat flux model, *Physics Letters A,* Vol. 383, No. 2, pp. 276-281, 2019/01/12/, 2019.

[40] M. Turkyilmazoglu, An analytical treatment for the exact solutions of MHD flow and heat over two–three dimensional deforming bodies, *International Journal of Heat and Mass Transfer,* Vol. 90, pp. 781-789, 2015/11/01/, 2015.

[41] R. Ellahi, S. Alamri, A. Majeed, Effects of MHD and slip on heat transfer boundary layer flow over a moving plate based on specific entropy generation, *Journal of Taibah University for Science,* Vol. 12, pp. 1-7, 06/14, 2018.

[42] K. Sharma, N. Vijay, O. Makinde, S. B. Bhardwaj, F. Mabood, Boundary layer flow with forced convective heat transfer and viscous dissipation past a porous rotating disk, *Chaos Solitons & Fractals,* Vol. 148, pp. 111055, 05/31, 2021.

[43] F. Ishtiaq, R. Ellahi, M. M. Bhatti, S. Sait, Convective heat transfer with Hall current using magnetized non-Newtonian Carreau fluid model on the cilia-attenuated flow, *International Journal of Numerical Methods for Heat & Fluid Flow,* Vol. 34, 07/16, 2024.

[44] S. O. Adesanya, E. O. Oluwadare, J. A. Falade, O. Makinde, Hydromagnetic natural convection flow between vertical parallel plates with time-periodic boundary conditions, *Journal of Magnetism and Magnetic Materials,* Vol. 396, 07/01, 2015.

[45] A. Zeeshan, M. Imran Khan, R. Ellahi, D. Asghar, Artificial neural network simulation and sensitivity analysis for optimal thermal transport of magnetic viscous fluid over shrinking wedge via RSM, *International Journal of Numerical Methods for Heat & Fluid Flow,* Vol. 33, 07/07, 2023.

[46] W. U. Hassan, K. Shabbir, A. Zeeshan, R. Ellahi, Regression analysis for thermal transport of fractional-order magnetohydrodynamic Maxwell fluid flow under the influence of chemical reaction using integrated machine learning approach, *Chaos, Solitons & Fractals,* Vol. 191, pp. 115927, 2025/02/01/, 2025.

[47] A. R. Ajaykumar, P. Kumar, F. Almeida, B. Nagaraja, Q. Al-Mdallal, Sensitivity analysis and response surface methodology for entropy optimization in the exponentially stretching stratified curved sheet for Casson–Williamson nanofluid flow, *International Journal of Thermofluids,* Vol. 22, pp. 100668, 2024/05/01/, 2024.

[48] A. Zeeshan, H. Javed, N. Shehzad, S. Sait, R. Ellahi, An integrated numerical and analytical investigation on cilia-generated MHD flow of Jeffrey fluid through a porous medium, *International Journal of Numerical Methods for Heat & Fluid Flow,* Vol. 34, 08/30, 2024.